THE DISCOVERY OF THE MOST DISTANT KNOWN TYPE IA SUPERNOVA AT REDSHIFT 1.914

David O. Jones[1], Steven A. Rodney[1,2], Adam G. Riess[1,3], Bahram Mobasher[4], Tomas Dahlen[3], Curtis McCully[5], Teddy F. Frederiksen[6], Stefano Casertano[3], Jens Hjorth[6], Charles R. Keeton[5], Anton Koekemoer[3], Louis-Gregory Strolger[7], Tommy G. Wiklind[8], Peter Challis[9], Or Graur[10,11], Brian Hayden[12], Brandon Patel[5], Benjamin J. Weiner[13], Alexei V. Filippenko[14], Peter Garnavich[12], Saurabh W. Jha[5], Robert P. Kirshner[9], Henry C. Ferguson[3], Norman A. Grogin[3], and Dale Kocevski[9]

ABSTRACT

We present the discovery of a Type Ia supernova (SN) at redshift $z = 1.914$ from the CANDELS multi-cycle treasury program on the *Hubble Space Telescope (HST)*. This SN was discovered in the infrared using the Wide-Field Camera 3, and it is the highest-redshift Type Ia SN yet observed. We classify this object as a SN Ia by comparing its light curve and spectrum with those of a large sample of Type Ia and core-collapse SNe. Its apparent magnitude is consistent with that expected from the ΛCDM concordance cosmology. We discuss the use of spectral evidence for classification of $z > 1.5$ SNe Ia using *HST* grism simulations, finding that spectral data alone can frequently rule out SNe II, but distinguishing between SNe Ia and SNe Ib/c can require prohibitively long exposures. In such cases, a quantitative analysis of the light curve may be necessary for classification. Our photometric and spectroscopic classification methods can aid the determination of SN rates and cosmological parameters from the full high-redshift CANDELS SN sample.

1. INTRODUCTION

Over the past decade, measurements of Type Ia supernovae (SNe) at redshift $z \gtrsim 1$ have extended the observed population to a time when the universe was matter dominated (Riess et al. 2001, 2004, 2007; Suzuki et al. 2012; Rodney et al. 2012; Rubin et al. 2013). At these lookback times of $\gtrsim 7\,\mathrm{Gyr}$, the predicted effects of dark energy are small, while the typical conditions under which SNe form are increasingly different from local environments.

These characteristics may allow observations at high redshift to constrain an evolutionary change in SN Ia brightness independent of our understanding of dark energy. This type of systematic shift in magnitude could be caused by changing metallicity or progenitor masses (e.g., Domínguez et al. 2001). Such an effect could be present at a lower level in intermediate-redshift SN samples ($0.2 \lesssim z \lesssim 1.0$), and therefore be a source of uncertainty in the determination of the dark energy equation-of-state parameter ($w = P/(\rho c^2)$; Riess & Livio 2006).

Observations of high-redshift SNe Ia could also place constraints on the binary companions of SN progenitors. The two most likely SN Ia progenitor models are the single-degenerate scenario, where a white dwarf accretes matter from a main-sequence or giant companion, and the double-degenerate scenario, where SNe occur through the merging of two carbon-oxygen (C-O) white dwarfs. A substantial difference between these mechanisms, however, is the typical time interval from progenitor formation to explosion; progenitors would likely take $\gtrsim 10^9$ yr to reach the Chandrasekhar limit by mass transfer from a nondegenerate companion, but would more often take less time in a system of two C-O white dwarfs (for a recent review of SN Ia progenitors, see Wang & Han 2012). The distribution of times between formation and explosion, known as the delay-time distribution (DTD), can therefore be used to set constraints on SN progenitor models. Observations of SN rates measure the convolution of the DTD with the cosmic star-formation history, and high-redshift rates are the most sensitive to delay times (Strolger et al. 2010; Graur et al. 2011).

Due to the high sensitivity and angular resolution of the *Hubble Space Telescope (HST)*, its Advanced Camera for Surveys (ACS) has been the most effective instrument for observing and monitoring SNe out to $z \approx 1.5$. To find SNe at higher redshifts in the rest-frame optical, where they are brightest and we understand them best, searching in the near-infrared (IR) with the recently installed Wide-Field Camera 3 (WFC3) allows SN surveys to reach unprecedented depths not accessible from the ground (F160W limiting Vega magnitude ~ 25.5, equal to the peak observed brightness of a typical SN Ia at $z \approx 2.5$).

In this paper we present observations of a SN Ia at

[1] Department of Physics and Astronomy, The Johns Hopkins University, Baltimore, MD 21218.
[2] Hubble Fellow.
[3] Space Telescope Science Institute, Baltimore, MD 21218.
[4] Department of Physics and Astronomy, University of California, Riverside, CA 92521.
[5] Department of Physics and Astronomy, Rutgers, The State University of New Jersey, Piscataway, NJ 08854.
[6] Dark Cosmology Centre, Niels Bohr Institute, University of Copenhagen, Juliane Maries Vej 30, DK-2100 Copenhagen, Denmark.
[7] Department of Physics, Western Kentucky University, Bowling Green, KY 42101.
[8] Joint ALMA Observatory, ESO, Santiago, Chile.
[9] Harvard/Smithsonian Center for Astrophysics, Cambridge, MA 02138.
[10] School of Physics and Astronomy, Tel-Aviv University, Tel-Aviv 69978, Israel.
[11] Department of Astrophysics, American Museum of Natural History, Central Park West and 79th Street, New York, NY 10024-5192.
[12] Department of Physics, University of Notre Dame, Notre Dame, IN 46556.
[13] Department of Astronomy, University of Arizona, Tucson, AZ 85721.
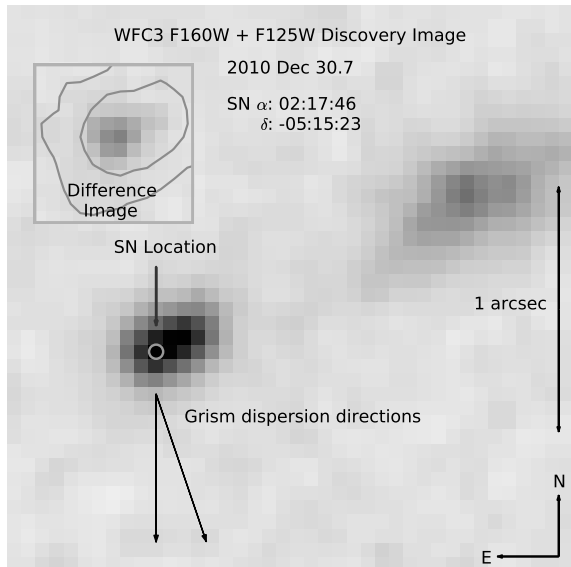[14] Department of Astronomy, University of California, Berkeley, CA 94720-3411.

FIG. 1.— The WFC3 F160W + F125W discovery and difference images (using a late-time, SN-free template) for SN UDS10Wil. The SN is located $\sim 0''.1$ from the center of the host galaxy (2 ACS pixels). The contours plotted on the difference image of the SN (upper left) show the regions containing 68% and 95% of the host galaxy light. The center of the nearest neighboring galaxy, which causes minimal lensing of the SN (see §4.1), is located $\sim 1''.5$ away.

$z = 1.91$ (SN UDS10Wil), the highest-redshift SN Ia discovered to date. It was found in the Cosmic Assembly Near-infrared Deep Extragalactic Legacy Survey (CANDELS, PI: Faber & Ferguson; Grogin et al. 2011; Koekemoer et al. 2011). The full CANDELS SN sample is designed to measure SN rates and to study SN systematics at redshifts greater than 1.5. Similar to SN Primo, a $z = 1.55$ WFC3-discovered SN (Rodney et al. 2012; Frederiksen et al. 2012), UDS10Wil also has spectroscopic evidence for classification. We present the discovery of SN UDS10Wil in §2. Section 3 discusses its classification from photometry and *HST* grism spectroscopy. In §4 we estimate the brightness correction due to gravitational lensing and fit the light curve. We discuss our results and the *HST* spectral classification in §5, and our conclusions are given in §6.

2. DISCOVERY

SN UDS10Wil was discovered in the second epoch of CANDELS observations of the UKIDSS Ultra-Deep Survey field (UDS; Lawrence et al. 2007; Cirasuolo et al. 2007) on 2010 December 30, after subtracting the images obtained in the first epoch (2010 November 11). It was detected at high significance in both F160W and F125W difference images, while a flux decrement was seen at the same location in the ACS filter F814W difference image (detected at $\sim 2.5\sigma$). The SN searching is performed by eye in the difference images, and in this case we could only subtract the first epoch of UDS observations (50 days before) from the second epoch, as no earlier WFC3 data were available. The F814W flux decrement suggests that pre-maximum SN light was present in the first epoch of UDS observations. Thus, the SN was brighter in the pre-maximum, shorter-wavelength ACS imaging.

The WFC3 (F125W + F160W) discovery-epoch image of SN UDS10Wil is shown in Figure 1, using a late-time (2011 December), SN-free template for the difference imaging. The J2000 SN coordinates are $\alpha = 02^\mathrm{h}17^\mathrm{m}46^\mathrm{s}$, $\delta = -05°15'23''$. It was $\sim 0''.1$ from the center of its host galaxy (~ 2 ACS pixels, ~ 0.9 kpc in distance), making it highly probable that this galaxy was the host and unlikely that the object was an active galactic nucleus.

At the time of discovery, we determined the photometric redshift of the host galaxy to be > 1.5, although this was measured before SN-free WFC3 host-galaxy images were available. At this redshift, the SN colors (F160W − F814W 3σ upper limit, and F125W − F160W) were consistent with those expected for a SN Ia at $z > 1.5$ and inconsistent with a core-collapse (CC) SN, so we triggered follow-up observations with the X-shooter spectrograph on the ESO Very Large Telescope (VLT) to obtain a spectroscopic redshift of the host.[15]

Moreover, we monitored the SN with the *HST* SN Multi-Cycle Treasury follow-up program (GO-12099; PI: Riess). We imaged the SN with *HST* (20 orbits, to obtain the light curve as well as SN-free template observations) and we obtained G141 grism spectroscopy (15 orbits, for resolution $R \approx 130$).

To measure the photometry of the SN, we subtracted the late-time template images from the UDS/SN follow-up observations. We measured the flux within a fixed aperture of 3-pixel radius and estimated errors in the flux from the sky noise of the nearby background-subtracted image. Details of the *HST* observations are listed in Table 1, and the grism spectrum is discussed along with the SN classification in §3.2.

2.1. *Redshift*

We remeasured the spectral energy distribution (SED) of the SN UDS10Wil host galaxy, including photometry from late-time WFC3 and ACS templates as well as Subaru, UKIRT, and IRAC data. The Balmer break is between the Subaru z band and the WFC3 J band, making the most likely redshift between 1.8 and 2.2 (see the lower-left panel of Fig. 3). Using the X-shooter spectrum, we narrowed this result by identifying [O II] and [O III] doublets in the host-galaxy spectrum, giving a precise redshift of 1.914.

The result is also consistent with the *HST* G141 grism spectrum, which contains a clear detection of [O III] $\lambda\lambda4959, 5007$. However, the grism spectrum cannot resolve the doublet, as the spectrum is convolved with both the shape of the host galaxy and the point-spread function (PSF; combined full width at half-maximum intensity $\sim 116\,\text{Å}$) and sampled at a resolution of only $46.5\,\text{Å}\,\text{pixel}^{-1}$. The VLT spectrum, along with an analysis of the late-type host galaxy of SN UDS10Wil, will be presented by Frederiksen et al. (in preparation).

3. CLASSIFICATION

We classified SN UDS10Wil by analyzing its light curve and spectrum, informed by the host redshift. As detailed below, we first examined the light curve, finding

TABLE 1
Photometric Observations

UT Date	MJD	Filter	Exposure Time	Flux (counts s^{-1})	Vega Mag
2010 Nov. 08.8	55508.1	F814W	3517.0	0.143 ± 0.054	27.635 ± 0.413
2010 Nov. 11.2	55511.2	F160W	1605.8	0.517 ± 0.074	25.221 ± 0.156
2010 Nov. 11.2	55511.2	F125W	955.9	0.698 ± 0.096	25.535 ± 0.149
2010 Dec. 28.0[*]	55557.4	F814W	3817.0	-0.063 ± 0.041	...
2010 Dec. 30.7[*]	55560.7	F160W	1705.9	1.22 ± 0.079	24.290 ± 0.070
2010 Dec. 30.8[*]	55560.8	F125W	955.9	1.403 ± 0.102	24.776 ± 0.079
2011 Jan. 12.6	55573.6	F160W	3617.6	0.901 ± 0.063	24.616 ± 0.076
2011 Jan. 12.8	55573.8	F125W	3617.6	0.759 ± 0.062	25.443 ± 0.089
2011 Jan. 13.6	55574.6	F850LP	1994.0	-0.018 ± 0.035	...
2011 Jan. 23.4	55584.3	F160W	3667.6	0.780 ± 0.061	24.774 ± 0.085
2011 Jan. 23.4	55584.4	F125W	3867.6	0.535 ± 0.059	25.823 ± 0.118
2011 Feb. 04.2	55596.1	F160W	3767.6	0.441 ± 0.061	25.392 ± 0.150
2011 Feb. 04.2	55596.1	F125W	3717.6	0.437 ± 0.062	26.043 ± 0.154
2011 Feb. 16.1	55608.1	F160W	4973.5	0.309 ± 0.058	25.779 ± 0.205
2011 Feb. 16.3	55608.2	F125W	4973.5	0.183 ± 0.057	26.989 ± 0.337
2011 Jan. 12.7	55573.7	G141	39088.0	(grism obs)	...

[*] Discovery epoch.

that it is consistent only with a SN Ia. In particular, the combination of its early-time colors with its rapid late-time decline rate does not agree with CC SN models. We then used the spectrum to independently rule out SNe II. While the spectral absorption features alone are unable to convincingly distinguish between a SN Ia and a SN Ib/c, SNe II have features that are inconsistent with the data (see Filippenko 1997 for a review of SN spectra).

3.1. Photometric Classification

To classify SN UDS10Wil we compared the observed UDS10Wil light curve against Monte Carlo simulations of Type Ia and CC SNe at redshift 1.91, generated with the SuperNova ANAlysis software (SNANA[16]; Kessler et al. 2009b). We used a least-squares fit to scale the magnitude of the simulated light curves to match our data, thus allowing us to examine how our data compare to the shapes and colors of simulated SNe while removing any assumptions on cosmology or intrinsic SN luminosity. We then measured the χ^2 statistic for each simulated SN compared to our data and converted these χ^2 values into a Type Ia SN classification probability using a simple Bayesian framework, similar to Poznanski et al. (2007), Kuznetsova & Connolly (2007), and Sako et al. (2011). The full Bayesian formalism, along with a description of the simulations and our Bayesian priors, is presented in the Appendix.

Our procedure gives us a very high probability that SN UDS10Wil is a SN Ia. As such, varying our priors on parameters such as shape, color, A_V, R_V, or SN rates has a very minor effect on the outcome. The reliance on only 43 CC SN templates constitutes the greatest uncertainty in our procedure. However, using a classification procedure very similar to ours, Sako et al. (2011) found that classification using only 8 CC SN templates still returns SN Ia classification purities of $\gtrsim 90\%$.

We find that the probability of a SN Ia was 99.98%, with a SN Ib/c probability of 2.1×10^{-4} (ruled out at $\sim 3.7\sigma$) and a SN II probability of 1.0×10^{-7} (ruled out at

$\sim 5.3\sigma$). This indicates that the Type Ia model dominates the probability calculation, and no CC SN models can adequately describe the observed photometric data.

Figure 2 shows the best-fit light curves, along with the flux range of simulated SN light curves encompassing 95% of the Bayesian evidence for each SN type. The best-fit light curves for Types Ia, Ib/c, and II SNe return χ^2/ν values of 18.6/11, 35.5/11, and 51.1/11, respectively. Note that these χ^2 values are only illustrative of the quality of the match for each model. They represent the best match from a large but limited number of random simulations, so one cannot use these values in χ^2 goodness-of-fit tests for model rejection. By contrast, the final classification probability relies on the weight of evidence from all realizations of each model.

Our best-fit x_1 and C values for the Type Ia model were -1.56 and -0.12, respectively. These values are fully consistent with the SALT2 parameters derived from light-curve fitting in §4.2 ($x_1 = -1.50 \pm 0.51$ and $C = -0.07 \pm 0.11$). We note that if we increase the errors such that the SN Ia $\chi^2/\nu \approx 1$ (accounting for the possibility that we underestimated the uncertainties), the Type Ia probability is still as high as 99.84%. Figure 2 shows that the nearly 100% probability of classification as a SN Ia (and the superior best-fit χ^2 value) arises because the SN Ib/c and SN II light-curve fits are unable to match the combination of SN UDS10Wil's high signal-to-noise ratio (S/N) discovery-epoch colors and its rapid light-curve decline rate.

As a verification of this light-curve classification, we used the Photometric SuperNova IDentification software (PSNID; Sako et al. 2008), finding that it also prefers a SN Ia with a slightly higher 4.1σ confidence. The difference in probability is primarily due to our conservative CC model uncertainties (see the Appendix), which reduce the χ^2 values of CC SNe. Although it only uses 8 CC SNe, the purity of PSNID classifications has been robustly tested using Sloan Digital Sky Survey (SDSS) SNe, and it obtained the highest figure of merit in the SN Photometric Classification Challenge (Kessler et al. 2010).

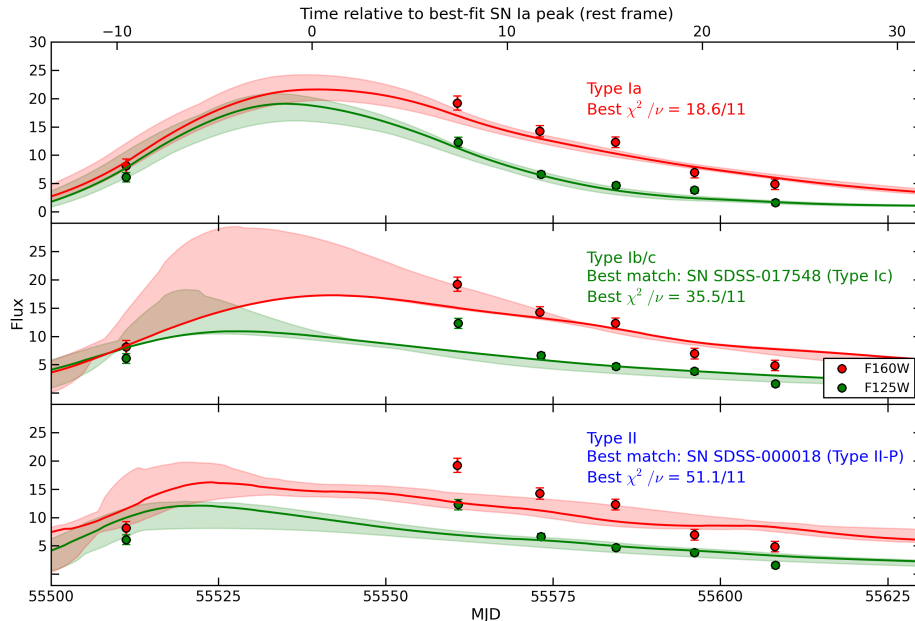[16] http://sdssdp62.fnal.gov/sdsssn/SNANA-PUBLIC/.

Fig. 2.— The best-fit light curves using SNANA-simulated Type Ia, Type Ib/c, and Type II SNe (top to bottom). Red and green colors indicate photometry and simulations for the F160W and F125W filters (approximately rest-frame B and V), respectively. Shaded regions include the range of SN fits that encompass 95% of the Bayesian evidence for a given SN type. Type Ib/c and Type II fits have higher χ^2 values (even including model uncertainties), due to their inability to match the combination of the colors nearest to maximum light and the rapid rate of decline. The sum of the evidence for a SN Ia model gives a nearly 100% probability that the SN is of Type Ia. We included F814W and F850LP data in the χ^2 fitting, but have omitted them in this figure for visual clarity. The fluxes shown are transformed from Vega magnitudes using a zeropoint of 27.5.

3.2. Spectrum

Spectroscopic confirmation of SNe has proven challenging at these redshifts (see the discussions in Rodney et al. 2012 and Rubin et al. 2013), due to the difficulty of obtaining high S/N observations and the paucity of defining features in the available window (for UDS10Wil, ~ 1.12–$1.65\,\mu$m; rest frame ~ 3840–5660 Å). In the case of SN UDS10Wil, the SN was separated from its host galaxy by only $\sim 0''.1$, contaminating the SN spectrum with host-galaxy light. We removed the host galaxy from the spectrum by subtracting a section of the galaxy free from SN light, but the combined noise from the SN and host-galaxy spectra made a spectral classification inconclusive, even with substantial host-galaxy smoothing.

As an alternative approach that avoids adding additional host-galaxy noise to the SN spectrum, we generated a noise-free synthetic host spectrum. We fit SEDs, using a library of spectral templates, to optical and near-IR Subaru, ACS, WFC3, and UKIRT host-galaxy photometry following Dahlen et al. (2010). We then simulated the observed grism host spectrum with the aXeSim software package.[17] The aXeSim software convolves the SED with the shape of the host galaxy and *HST* PSF and samples the spectrum at the G141 spectral resolution of 46.5 Å pixel^{-1}.

One would not necessarily expect emission lines to be the same strength in the template as in the real galaxy due to its differing metallicity, star formation rate, and population of massive stars. Therefore, we replaced the pixels covering the [O III] line in our simulated host galaxy with those covering the prominent [O III] line

from the grism spectrum. We omitted these pixels (the shaded region in Fig. 3) when we later fit spectral templates to the SN spectrum, as we did not have a SN-free line measurement to subtract from the observations. We then rescaled the aXeSim output spectrum to match the F160W magnitude of the host galaxy as measured in the last epoch of follow-up imaging after the SN had faded. Our simulated host-galaxy spectrum is shown in Figure 3 (upper left).

After subtracting the host-galaxy model from the SN spectrum contaminated with host light, we used the Supernova Identification (SNID) code[18] from Blondin & Tonry (2007) to match the UDS10Wil spectrum with Type Ia, Type Ib/c, and Type II SN template spectra to determine the best-fit spectrum for each class. For SN Ia fits, we only used templates within ± 3 rest-frame days of the age of the SN UDS10Wil spectrum. The age is based on the SALT2 fit in §4.2, which gives $\sim 12 \pm 1$ day after maximum (rest frame). For CC SN fits, we used any templates which put the time of maximum between the first two epochs of observation (the same as our prior in §3.1). When fitting the spectrum to templates, SNID removes the continuum using a high-order polynomial fit and only matches the spectral features, making the fit independent of reddening and brightness.

SNID returns the $r$lap parameter, which is meant to quantify the quality of the correlation (see Blondin & Tonry 2007 for details). Blondin & Tonry (2007) suggest that $r$lap values less than 5 are inconclusive. Note that SNID does not apply a broadening symmetric function

---

[17] http://axe.stsci.edu/axesim/.

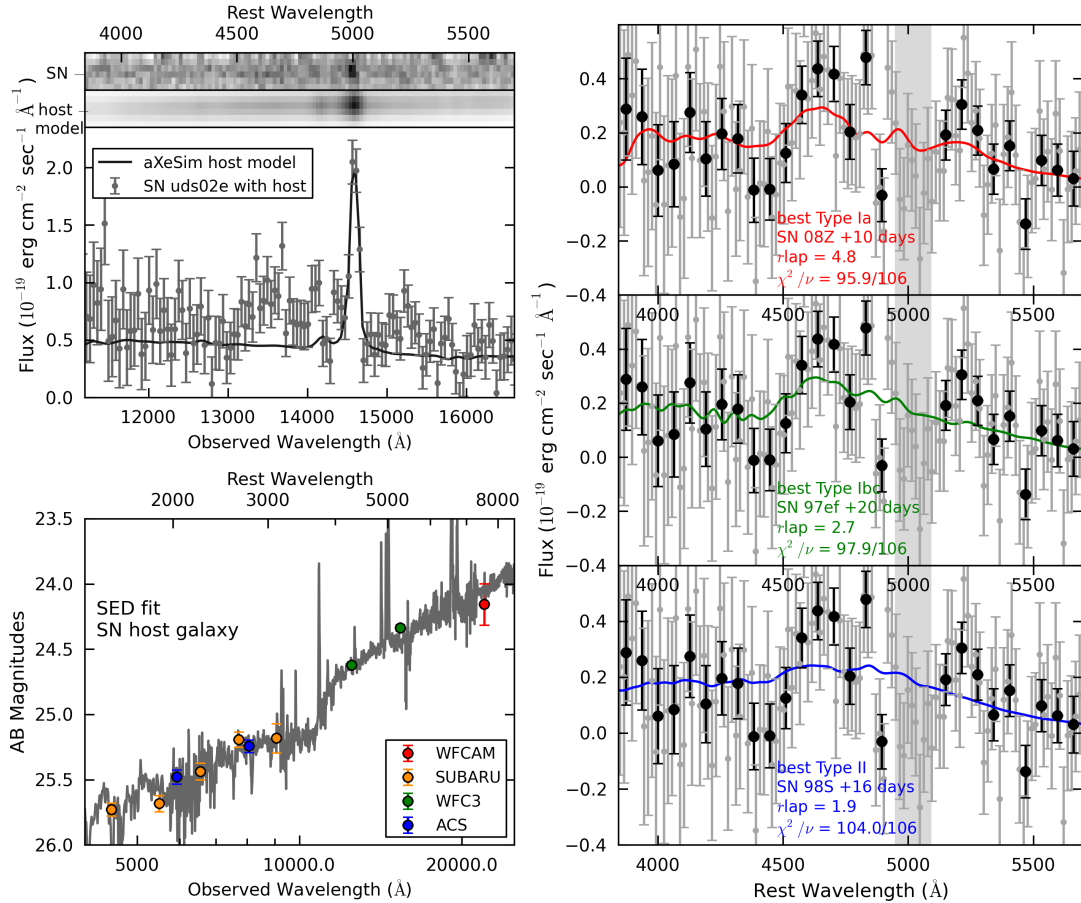[18] http://www.oamp.fr/people/blondin/software/snid/index.html.

FIG. 3.— The spectrum of SN UDS10Wil, from which the host-galaxy light has been subtracted using a spectrum fit to the host's SED. The host SED and its best-fit spectral template is shown at the bottom left. The two-dimensional and one-dimensional grism spectrum along with the simulated host-galaxy spectrum (the SED convolved with the shape of the host using aXeSim) are given at the upper left. On the right we show the best-fit SN templates from SNID for Types Ia, Ib/c, and II. We illustrate median bins to visually emphasize the spectral features, but have used the unbinned data for our analysis. Although the spectrum can be fit reasonably well by both a SN Ia or a SN Ib/c, a SN II does not contain the spectral features seen at ~ 4600 and ~ 5200 Å in the rest frame. Data in the [O III] subtraction region (the shaded region) were not used in the fit.

(Tonry & Davis 1979), which should be used when the widths of SN features are comparable to the resolution of the spectrum. As the rest-frame G141 resolution is ~ 16 Å pixel^{-1} and significant SN features have a typical width ~ 50 Å, this is not a major concern. However, the inclusion of this function for grism data could improve future SNID classifications, especially those at lower redshift.

The right side of Figure 3 shows the best-fit Type Ia, Ib/c, and II SN templates with $r$lap values of 4.8, 2.7, and 1.9, respectively. We show median bins to emphasize the spectral features, but we fit spectra to the unbinned data. The data can be fit by 6 other normal SNe Ia with $r$lap values of at least 4. Five other SN Ib/c fits have an $r$lap of at least 2, and only two other SN II fits have an $r$lap of greater than 1.5.

The χ^2 values for the fits, now including continuum, to Type Ia, Ib/c, and II SNe are 95.9, 97.9, and 104.0 (respectively) with 106 degrees of freedom. We note that both SNe Ia and SNe Ib/c can provide good fits, although the former give a slightly better match. However, all SN II templates yield a poor correlation; the rest-frame features at ~ 4600 and ~ 5200 Å (which are created by neighboring Fe II, Fe III, Si II, and S II absorption in

SNe Ia; Filippenko 1997) are not well fit by the spectra of SNe II. We note that although not all of the SNID SNe II are as featureless as the best-fit spectrum shown in Figure 3, they all have difficulty matching the strength or location of the spectral features. Even Type II-P templates, which typically have stronger features, have a maximum $r$lap of only 1.4.

Because the best $r$lap value is less than 5, this SN cannot be considered to be spectroscopically confirmed. In addition, the "lap" parameter, which describes the overlap in wavelength space between the template and SN spectrum, is 0.39 for each of the best-fit SN Ia and CC SN templates. This is below the minimum lap of 0.4 used by Blondin & Tonry (2007) for spectral confirmation. However, the SN UDS10Wil spectrum still favors classification as a SN Ia and its $r$lap is comparable to that of other high-redshift SNe Ia. SN Primo (Rodney et al. 2012; $z = 1.55$) had an $r$lap of only 3.7. We also fit the spectrum of SN SCP-0401 (Rubin et al. 2013; $z = 1.71$), finding that it is best matched by featureless SNID Type Ia and Type Ib/c spectra. However, if we require a match to at least one spectral feature or a lap value greater than 0.1, the maximum SN Ia $r$lap is 4.6 (SN 1993ac, +7 days; lap of 0.2). SNID templates begin at $\lambda_{\rm rest} = 2500$ Å, so

the first $\sim 500\,\text{Å}$ of the SN SCP-0401 spectrum were not included in the SNID fit.

4. ANALYSIS

Taken together, the photometric evidence suggests that UDS10Wil is a SN Ia with high confidence. The spectroscopic evidence independently favors a Type Ia classification. We now proceed to derive its shape and color-corrected magnitude, taking into account the possibility that the SN light has been gravitationally lensed by foreground structure.

4.1. *Lensing*

Our ability to use SNe Ia as accurate distance indicators to constrain cosmological parameters requires us to determine the impact of foreground-matter inhomogeneities on the flux of the SN (e.g., Jönsson et al. 2006). Even without multiple images, gravitational lensing can significantly magnify the SN, altering our measurement of its distance. SN UDS10Wil is close in projection to another galaxy (see Fig. 1) separated by only $1''.54$. Therefore, it is necessary to estimate the possible magnification of the SN which could lead to a bias in the derived SN Ia distance. All other foreground sources are greater than $4''.5$ away and cause negligible magnification.

We fit the SED of the lens galaxy as described by Wiklind et al. (2008) to characterize its physical properties. We used a Chabrier initial mass function (IMF; Chabrier 2003) rather than the Salpeter IMF cited by Wiklind et al. (2008); the former gives a slightly smaller stellar mass but is a more accepted model. To account for photometric uncertainties, we drew Monte Carlo samples for the measured photometry of the galaxy and used the best-fitting SED models to characterize the SED. The SED fit indicates a low-mass galaxy with a photometric redshift 0.283 ± 0.080 and a stellar mass $\log(M_\star/M_\odot) = 7.968 \pm 0.222$. We used these parameters to create a plausible mass model of the galaxy and estimate the magnification of the SN.

We modeled the stellar component of the galaxy as an exponential disk using parameters measured from GAL-FIT (Peng et al. 2002) and the dark-matter halo using a Navarro-Frenk-White (NFW) profile (Navarro et al. 1997). We used the broken power law given by Yang et al. (2012) to relate the stellar mass M_* to the halo mass and the mass-concentration relation given by Macciò et al. (2008) when modeling the halo.

Both the mass-concentration and stellar-to-halo mass relations have significant scatter around the median relations. To account for this scatter, we took 10,000 Monte Carlo realizations of lensing potentials to calculate the expected magnification distribution. We also drew a photo-z and stellar mass distribution from the Monte Carlo realizations of our SED fits.

Despite the proximity of the galaxy, its low mass makes magnification a minor effect. The median magnification from the above analysis is $2.8^{+2.3}_{-1.2}\%$, where the lower and upper uncertainties represent the 16$^{\text{th}}$ and 84$^{\text{th}}$ percentiles ($\pm 1\sigma$), respectively. These models do assume a spherical NFW profile, but adding ellipticity to the halo does not significantly change our results. This analysis shows that the systematic offset due to lensing is much smaller than the photometric uncertainties; we applied the lensing correction to our derived magnitude, but it does not have a significant effect on our distance modulus.

4.2. *Light-curve Fit*

We fit the light curve using the SALT2 implementation (Guy et al. 2010) contained in SNANA (Fig. 4). Note that although the ACS data provide a valuable color constraint for classification purposes, we have omitted them from our cosmological analysis. At $z = 1.914$, the ACS bands sample rest-frame wavelengths of 2400–3300 Å, where SNe Ia are more heterogeneous (Ellis et al. 2008) and may evolve with redshift (Foley et al. 2012). Furthermore, the rest-frame UV has been problematic for SN Ia light-curve fitters (Kessler et al. 2009a). Given these concerns, we discarded the ACS data for our light-curve fitting in order to avoid introducing a bias in the derived distance. The ACS observations provided only a single measurement with positive flux (F814W at MJD = 55801.1), so this does not exclude a large fraction of useful data.

The light-curve parameters for SN UDS10Wil are typical of SNe Ia; we derive values of $x_1 = -1.50 \pm 0.51$ and $C = -0.071 \pm 0.11$, which are consistent with the parameters described by Kessler et al. (2009a) ($\bar{C} = 0.04$, $\sigma_C = 0.13$, $\bar{x}_1 = -0.13$, $\sigma_{x_1} = 1.24$). SNANA also gives a peak magnitude $m_B^* = 26.20 \pm 0.11$. We then converted our SALT2 values into SiFTO values (Conley et al. 2008), using the relations of Guy et al. (2010), in order to use the shape and color constants from SNLS ($\alpha = 1.367$, $\beta = 3.179$; Sullivan et al. 2011). We derived a light-curve shape and color-corrected magnitude (m_{corr}) using

$$m_{\text{corr}} = m_B^* + \alpha \times (s-1) - \beta \times C, \qquad (1)$$

where m_{corr} is equal to the distance modulus plus the SN absolute magnitude, M. Here m_B^* is the peak SN magnitude, s is the SiFTO stretch parameter, and C describes the color; also, m_B^* includes the lensing correction of $0.030^{+0.024}_{-0.013}$ mag.

This analysis gives a corrected magnitude of 26.15 ± 0.39. We compare to the corrected magnitude for ΛCDM, $m_{\Lambda CDM}$, by using the cosmological parameters from Sullivan et al. (2011) ($\Omega_\Lambda = 0.73$, $\Omega_M = 0.27$, $w = -1$, $H_0 = 71.6\,\text{km}\,\text{s}^{-1}\,\text{Mpc}^{-1}$) and a least-squares fit to the Conley et al. (2011) SNe. We added an offset of 0.27 mag to the value of m_B for the Conley et al. (2011) SNe in order to match the normalization of the SALT2 fitter contained in SNANA, finding $m_{\Lambda CDM} = 26.46$ mag (including the offset, this gives an absolute SN magnitude $M = -19.39$). SN UDS10Wil is less than 1σ from ΛCDM.

We also fit the light curve with MLCS (Jha, Riess, & Kirshner 2007), after using SDSS SNe to determine, and correct for, the m_{corr} offset between MLCS and SALT2 fits. MLCS gives the same corrected magnitude with a somewhat smaller uncertainty, $m_{\text{corr}} = 26.15 \pm 0.27$ mag (with $\Delta = 0.30 \pm 0.18$ and $A_V = 0.01 \pm 0.05$ mag). This value is slightly brighter than expected from ΛCDM, but consistent at 1.15σ. We verified that the MLCS and SALT2 parameters are consistent with each other using relations from Kessler et al. (2009a).
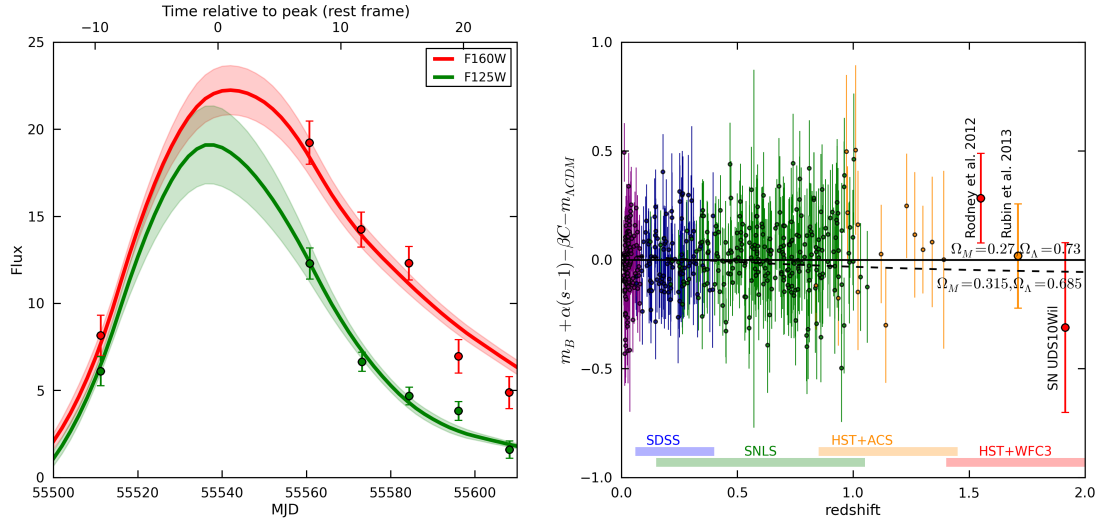
FIG. 4.— On the left, the SALT2 light-curve fit to SN UDS10Wil. SALT2 gives a normal set of light-curve parameters along with a corrected magnitude of 26.15 ± 0.39 (consistent with ΛCDM) and a reduced χ^2 of 1.5. On the right, we place SN UDS10Wil on the Hubble residual diagram using cosmological parameters from Sullivan et al. (2011) and $H_0 = 71.6 \, \mathrm{km \, s^{-1} \, Mpc^{-1}}$. For comparison, we also show the compilation of ~ 500 SNe from Conley et al. (2011). Lastly, using Sullivan et al. (2011) values for α and β, we include the other two SNe Ia with spectroscopic evidence for classification discovered at a redshift greater than 1.5 (Rodney et al. 2012; Rubin et al. 2013). The dotted line indicates the difference in $m_{\Lambda CDM}$ when using the recent cosmological parameters from the Planck collaboration ($\Omega_\Lambda = 0.685$, $\Omega_M = 0.315$; Planck Collaboration et al. 2013).
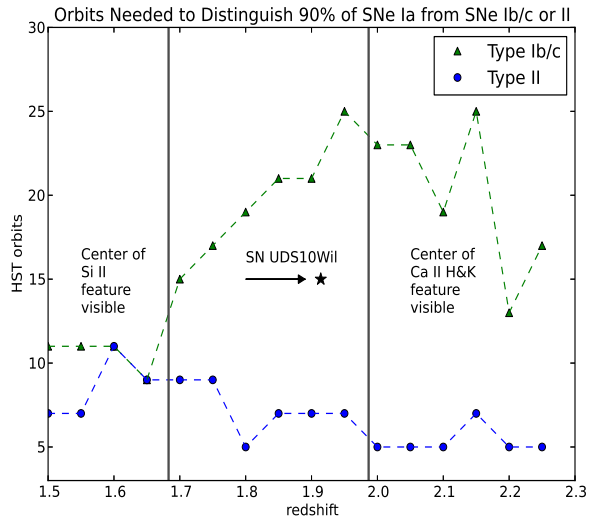

FIG. 5.— The number of orbits necessary to rule out the possibility of a SN II or SN Ib/c 90% of the time when observing a SN Ia. Using aXeSim, we simulated a variety of exposure times in the redshift range 1.5–2.3. We found that $\sim$5–10 orbits can rule out a SN II, but that the number of orbits required to rule out a SN Ib/c possibility is significantly greater. The number of orbits to rule out a SN Ib/c is much lower in the region where Si II and Ca II H&K are completely visible. These results indicate the need for photometric evidence in SN Ia classification at high redshift, although the *HST* grism can also be valuable in determining SN redshifts.

5. DISCUSSION

The observations of SN UDS10Wil presented here demonstrate that the *HST* WFC3 now allows the cosmological study of SNe Ia at higher redshifts than ever before. The analysis presented above is enabled by the photometric classification methods we employ. However, SN science, especially cosmology, has in the past relied heavily on spectroscopic evidence for classification.

At $z > 1.5$, deriving a spectral classification with *HST* requires a large number of orbits to obtain a high S/N. In addition, the *HST* IR grisms cover a relatively small rest-frame wavelength range. In the case of SN UDS10Wil, the G141 grism wavelength range (~ 1.12–$1.65 \, \mu$m; rest frame ~ 3840–$5660 \, \text{Å}$) does not include either the Si II absorption at $\sim 6150 \, \text{Å}$ or the Ca II H&K trough at $\sim 3750 \, \text{Å}$, which are some of the deepest SN Ia features (the features have equivalent widths $\sim 100 \, \text{Å}$). This means that spectral classifications of high-redshift SNe using SNID will have lower-significance correlations with SN Ia template spectra, and thus often yield $r$lap values much less than the suggested minimum of 5 (Blondin & Tonry 2007).

Host-galaxy contamination can be a significant source of noise in high-z SN grism spectra. In this work we have used aXeSim to remove host-galaxy light from the SN+host spectrum. However, even in a situation where a SN is well separated from its host galaxy, spectral evidence alone may not be enough to unequivocally classify the SN as Type Ia. Figure 5 shows the number of *HST* orbits with the G141 IR grism that are needed for SNID to correctly distinguish a SN Ia from a SN Ib/c or a SN II 90% of the time, in the redshift range 1.5–2.3. For this figure, we used aXeSim to simulate 100 SN Ia observations per unit redshift with 2.6 ks per orbit, from 0 to 100 orbits (2-orbit intervals). The background flux was set to $95 \, \mathrm{e^- \, s^{-1}}$, and the simulated SN magnitude was fixed at the peak magnitude of SN Primo (an F160W Vega magnitude of 23.98; Primo was observed closer to maximum than UDS10Wil). Each simulated grism spectrum was then processed with SNID, and the classification was deemed correct if the best $r$lap for a SN Ia template was larger than the best SN Ib/c or SN II $r$lap (we allow $r$lap < 5).

Figure 5 shows that, similar to the case of SN UDS10Wil, ruling out a SN II possibility requires only

~5–10 orbits ($1.5 < z < 2.3$). For a large program like CANDELS, with 200 follow-up orbits and a desired sample of ~10 SNe, this is a feasible number. Ruling out a SN Ib/c, however, can require up to 25 orbits, becoming most costly at those redshifts where Si II and Ca II H&K are not completely visible. At very high redshift, such as $z \approx 2.2$–2.3, Figure 5 shows that the G141 exposure time required to distinguish a SN Ia from a SN Ib/c begins to drop. The value of spectroscopic confirmation for such high-redshift SNe may warrant the necessary investment of orbits, especially if additional high-value targets can be simultaneously observed within the grism field of view. We note that simulating CC SN observations shows that SNID can occasionally misclassify CC SNe as SNe Ia, an effect we have not taken into account in this analysis.

The G102 grism can also be useful for picking out features such as Si II and Ca II H&K in the redshift ranges where the G141 grism does not contain them. Unfortunately, the consequence of its more limited wavelength range (~ 0.8–1.15 μm; rest frame ~ 2750–3950 Å at $z = 1.91$) is that a SN Ib/c template is more likely to match a SN Ia G102 spectrum well.

HST grism spectroscopy can be good at determining SN redshifts or host-galaxy properties. However, for reliable SN classification, photometric evidence is often important. In the case of SN UDS10Wil we improved upon the photometric methods of Rodney et al. (2012) by introducing a quantitative Bayesian method that returns probabilities for each SN type. With both photometric and spectroscopic methods, we can be confident in our classification and subsequent analysis.

6. CONCLUSIONS

At a redshift of 1.914, SN UDS10Wil is the most distant SN Ia yet known. Classification of this SN rests on photometry and grism spectroscopy, which rules out the possibility of a CC SN. The spectral evidence alone disfavors the possibility of a SN II, while supporting a SN Ia or SN Ib/c hypothesis. The combined SN colors and rapid decline rate are inconsistent with a CC SN and in good agreement with a SN Ia model.

We find that SN UDS10Wil is not significantly lensed, and its light-curve fit (with SALT2) is consistent with ΛCDM. An alternative fit with MLCS (Jha et al. 2007) is slightly brighter than ΛCDM, but consistent at 1.15σ.

When the full analysis of the CANDELS SNe is complete and combined with the data from the Cluster Lensing and Supernova survey with Hubble (PI: Postman; Postman et al. 2012), we expect that SN UDS10Wil will be one of a sample of ~ 10 SNe Ia above a redshift of 1.5 to be found by these programs. This SN is an example of an object in a new area of SN cosmology, one which has only begun to be explored in the last few years with the advent of WFC3 on *HST* and one with unique classification challenges. However, with the full sample of SNe at redshift greater than 1.5, new limits on the evolution of dark energy, the DTD, and the evolution of the SN Ia population will become possible.

APPENDIX

PHOTOMETRIC CLASSIFICATION METHOD

We began our classification procedure by using SNANA (Kessler et al. 2009b) to generate a Monte Carlo simulation of 30,000 SNe at redshift 1.91. 10,000 simulated SNe Ia were based on the SALT2 model (Guy et al. 2010), with values of the shape parameter x_1 drawn uniformly in the range -3 to 3 and the color parameter C from -0.4 to 0.6. These ranges cover the observed distribution of SALT2 parameter values (Kessler et al. 2009a), and the C term accounts for both intrinsic SN color and host-galaxy extinction (Guy et al. 2007). The remaining 20,000 simulated SNe were split evenly between the two principal CC SN classes, with light curves based on 16 Type Ib/c and 27 Type II SN templates that comprise the SNANA non-SN Ia library (including subtypes Ib, Ic, II-P, IIn, and II-L). Host-galaxy reddening was applied to each simulated CC SN using $R_V = 3.1$, with a random draw of A_V in the range 0 to 7 mag using the Cardelli et al. (1989) reddening law. For both the SN Ia and the CC SN simulations we chose random values for the date of the light-curve peak, using a range spanning the first to the second epoch of UDS10Wil observations.

To compare each of the 30,000 synthetic light curves to the $N = 15$ photometric observations of SN UDS10Wil, we computed the χ^2 statistic given by

$$\chi^2 = \sum_{i=1}^{N} \frac{(F_{\mathrm{obs},i} - A \times F_{\mathrm{sim},i})^2}{\sigma_{\mathrm{obs},i}^2 + \sigma_{\mathrm{sim},i}^2}, \tag{A1}$$

where $F_{\mathrm{obs},i}$ and $\sigma_{\mathrm{obs},i}$ are the fluxes and uncertainties for each observation. Here $F_{\mathrm{sim},i}$ and $\sigma_{\mathrm{sim},i}$ are the fluxes and uncertainties (respectively) for a single simulated SN on each observation date. The variable A is a scaling parameter,

described below. For SNe Ia, most of their intrinsic variability can be described by the SALT2 model's shape and color parameters. Additional variability causes scatter about the Hubble diagram, and is given by Guy et al. (2010) as 8.7% in distance modulus. We treat this variability as approximately equal to the model uncertainty, which in flux space translates to $\sigma_{\text{simIa},i} = 0.08 A \times F_{\text{sim},i}$.

CC SNe have greater heterogeneity, such that our relatively small set of discrete templates cannot describe the entire population. By setting a nonzero $\sigma_{\text{simCC},i}$, our limited CC SN template library can more accurately represent this diverse class. Considering a similar problem, Rodney & Tonry (2009) estimated $\sigma_{\text{simCC},i}$ by measuring the flux difference between all possible pairwise comparisons of templates of the same subclass and taking the median. We classify SN UDS10Wil using more templates than Rodney & Tonry (2009), such that the CC SN population is better sampled and less uncertainty is present. However, we adopt their value of $\sigma_{\text{simCC},i} = 0.15 A \times F_{\text{sim},i}$ as a conservative estimate.

We next chose the optimal distance or absolute magnitude of every simulated SN, therefore removing the assumptions on cosmology and SN luminosity functions that are built into the SNANA simulations. Here we have multiplied $F_{\text{sim},i}$ by A, a free parameter that introduces a coherent flux scaling across all bands. We find a separate value for A with each of the 30,000 comparisons, using χ^2 minimization to match the simulated magnitudes to the data with the equation

$$A = \frac{\sum\limits_{i=1}^{N} F_{\text{sim},i} F_{\text{obs},i}/\sigma_{\text{obs},i}^2}{\sum\limits_{i=1}^{N} F_{\text{sim},i}^2/\sigma_{\text{obs},i}^2}. \tag{A2}$$

We then converted the measured χ^2 values into a Type Ia SN classification probability using a simple Bayesian framework, similar to Poznanski et al. (2007), Kuznetsova & Connolly (2007), and Sako et al. (2011). The *likelihood* that the data (D) match a simulated SN of type T_j with parameters $\boldsymbol{\theta}$ (shape x_1, color C for SN Ia or A_V for CC SN types, and time of maximum light) is given by

$$p(D|\boldsymbol{\theta}, T_j) = \frac{e^{-\chi^2/2}}{\prod\limits_{i=1}^{N} \sqrt{2\pi(\sigma_{\text{obs},i}^2 + \sigma_{\text{sim},i}^2)}}, \tag{A3}$$

where χ^2 is given in Equation 1. Multiplying by prior probability distributions for each of the model parameters then gives us the *posterior probability* for each point in parameter space, $p(\boldsymbol{\theta}|T_j)p(D|\boldsymbol{\theta}, T_j)$. As we are interested in model selection, not parameter estimation, we can marginalize over all of the nuisance parameters $\boldsymbol{\theta}$. Approximating the marginalization integral with a discrete sum, the probability of SN type T_j given the model is

$$p(D|T_j) = \sum\limits_{i=1}^{N_{\text{sim}}(T_j)} p(\boldsymbol{\theta}|T_j)p(D|\boldsymbol{\theta}, T_j)\delta\boldsymbol{\theta}. \tag{A4}$$

For SN Ia parameters x_1 and C, we applied Gaussian priors based on the values given by Kessler et al. (2009a) ($\bar{C} = 0.04$, $\sigma_C = 0.13$, $\bar{x}_1 = -0.13$, $\sigma_{x_1} = 1.24$). For the CC SNe parameter A_V, we used the Monte Carlo recipe provided by Riello & Patat (2005) and implemented by Dahlen et al. (2012) for a random galaxy orientation. The distribution is peaked at $A_V = 0$ mag and falls off quickly such that $A_V \gtrsim 3$ mag is very unlikely. We used a flat prior for the time of peak brightness.

Note that for computational efficiency we have used SNANA to sample the multi-dimensional model parameter space using a Monte Carlo simulation with uniform sampling distributions (instead of the more typical approach, using a grid of parameter values). Thus, we must approximate $\delta\boldsymbol{\theta}$ – the vector of step sizes along each dimension of parameter space – using the range over which each parameter is sampled:

$$\delta\boldsymbol{\theta} = \frac{1}{N_j} \prod\limits_{k=1}^{N_\theta} \Delta\theta_k, \tag{A5}$$

where $\Delta\theta_k$ is each range, N_j is the number of simulated SNe in the class (we used 10,000), and the product is over N_θ, the number of parameters θ for the model: 3 for SNe Ia (x_1, c, t_{pk}) and 2 for CC SNe (A_V, t_{pk}).

Lastly, we multiplied each model by a SN rate prior $P(T_j)$. This prior is the fraction of SNe at redshift 1.91 that we expect to be a given type. We began by adopting the rate measurement from Dahlen et al. (2008) for SNe Ia and the local rates from Li et al. (2011) for CC SNe. We scaled the CC SN rates according to the cosmic star-formation history of Hopkins & Beacom (2006) using the form of Cole et al. (2001) and a modified Salpeter IMF (Baldry & Glazebrook 2003). The normalized rates showed, as an estimate, that one could expect only $\sim 2\%$ of SNe at this redshift to be of Type Ia. The SN UDS10Wil host galaxy SED (§3.2) is consistent with a starburst galaxy, so it is possible that these average rates overestimate the SN Ia rate in this galaxy. In addition, SN rates are very uncertain at this redshift, and the Dahlen et al. (2008) rates at this redshift are consistent with 0 SNe Ia; however, we note that lowering this rates

prior by an order of magnitude still returns a classification probability greater than 99%. Thus the result is largely independent of the uncertainty in SN Ia rates.

Applying Bayes' theorem gives the final probability that SN UDS10Wil is of Type Ia:

$$p(Ia|D) = \frac{p(D|Ia)p(Ia)}{\sum_j p(D|T_j)p(T_j)}, \tag{A6}$$

where the summation is over Type Ia, Ib/c, and II SN models (T_j). In the case of SN UDS10Wil, our likelihood function is sufficiently narrow that the priors have only a minor effect. Thus, we found that allowing R_V, SALT2 parameters α and β, or parameter ranges to vary does not substantially alter the high probability that this SN is of Type Ia.

REFERENCES

Amanullah, R., Lidman, C., Rubin, D., et al. 2010, ApJ, 716, 712

Baldry, I. K., & Glazebrook, K. 2003, ApJ, 593, 258

Bazin, G., Palanque-Delabrouille, N., Rich, J., et al. 2009, A&A, 499, 653

Blondin, S., & Tonry, J. L. 2007, ApJ, 666, 1024

Cardelli, J. A., Clayton, G. C., & Mathis, J. S. 1989, ApJ, 345, 245

Chabrier, G. 2003, PASP, 115, 763

Cirasuolo, M., McLure, R. J., Dunlop, J. S., et al. 2007, MNRAS, 380, 585

Cole, S., Norberg, P., Baugh, C. M., et al. 2001, MNRAS, 326, 255

Conley, A., Sullivan, M., Hsiao, E. Y., et al. 2008, ApJ, 681, 482

Conley, A., Guy, J., Sullivan, M., et al. 2011, ApJS, 192, 1

Dahlen, T., Mobasher, B., Dickinson, M., et al. 2010, ApJ, 724, 425

Dahlen, T., Strolger, L.-G., & Riess, A. G. 2008, ApJ, 681, 462

Dahlen, T., Strolger, L.-G., Riess, A. G., et al. 2004, ApJ, 613, 189

—. 2012, ApJ, 757, 70

Domínguez, I., Höflich, P., & Straniero, O. 2001, ApJ, 557, 279

Ellis, R. S., Sullivan, M., Nugent, P. E., et al. 2008, ApJ, 674, 51

Filippenko, A. V. 1997, ARA&A, 35, 309

Foley, R. J., Filippenko, A. V., Kessler, R., et al. 2012, AJ, 143, 113

Frederiksen, T. F., Hjorth, J., Maund, J. R., et al. 2012, ApJ, 760, 125

Graur, O., Poznanski, D., Maoz, D., et al. 2011, MNRAS, 417, 916

Grogin, N. A., Kocevski, D. D., Faber, S. M., et al. 2011, ApJS, 197, 35

Guy, J., Astier, P., Baumont, S., et al. 2007, A&A, 466, 11

Guy, J., Sullivan, M., Conley, A., et al. 2010, A&A, 523, A7

Hopkins, A. M., & Beacom, J. F. 2006, ApJ, 651, 142

Jha, S., Riess, A. G., & Kirshner, R. P. 2007, ApJ, 659, 122

Jönsson, J., Dahlén, T., Goobar, A., et al. 2006, ApJ, 639, 991

Kessler, R., Bassett, B., Belov, P., et al. 2010, PASP, 122, 1415

Kessler, R., Becker, A. C., Cinabro, D., et al. 2009a, ApJS, 185, 32

Kessler, R., Bernstein, J. P., Cinabro, D., et al. 2009b, PASP, 121, 1028

Koekemoer, A. M., Faber, S. M., Ferguson, H. C., et al. 2011, ApJS, 197, 36

Kuznetsova, N. V., & Connolly, B. M. 2007, ApJ, 659, 530

Lawrence, A., Warren, S. J., Almaini, O., et al. 2007, MNRAS, 379, 1599

Li, W., Leaman, J., Chornock, R., et al. 2011, MNRAS, 412, 1441

Macciò, A. V., Dutton, A. A., & van den Bosch, F. C. 2008, MNRAS, 391, 1940

Navarro, J. F., Frenk, C. S., & White, S. D. M. 1997, ApJ, 490, 493

Peng, C. Y., Ho, L. C., Impey, C. D., & Rix, H.-W. 2002, AJ, 124, 266

Planck Collaboration, Ade, P. A. R., Aghanim, N., et al. 2013, ArXiv e-prints

Postman, M., Coe, D., Benítez, N., et al. 2012, ApJS, 199, 25

Poznanski, D., Maoz, D., & Gal-Yam, A. 2007, AJ, 134, 1285

Riello, M., & Patat, F. 2005, MNRAS, 362, 671

Riess, A. G., & Livio, M. 2006, ApJ, 648, 884

Riess, A. G., Nugent, P. E., Gilliland, R. L., et al. 2001, ApJ, 560, 49

Riess, A. G., Strolger, L.-G., Casertano, S., et al. 2007, ApJ, 659, 98

Riess, A. G., Strolger, L.-G., Tonry, J., et al. 2004, ApJ, 607, 665

Rodney, S. A., & Tonry, J. L. 2009, ApJ, 707, 1064

Rodney, S. A., Riess, A. G., Dahlen, T., et al. 2012, ApJ, 746, 5

Rubin, D., Knop, R. A., Rykoff, E., et al. 2013, ApJ, 763, 35

Sako, M., Bassett, B., Becker, A., et al. 2008, AJ, 135, 348

Sako, M., Bassett, B., Connolly, B., et al. 2011, ApJ, 738, 162

Strolger, L.-G., Dahlen, T., & Riess, A. G. 2010, ApJ, 713, 32

Sullivan, M., Guy, J., Conley, A., et al. 2011, ApJ, 737, 102

Suzuki, N., Rubin, D., Lidman, C., et al. 2012, ApJ, 746, 85

Tonry, J., & Davis, M. 1979, AJ, 84, 151

Wang, B., & Han, Z. 2012, NewAR, 56, 122

Wiklind, T., Dickinson, M., Ferguson, H. C., et al. 2008, ApJ, 676, 781

Yang, X., Mo, H. J., van den Bosch, F. C., Zhang, Y., & Han, J. 2012, ApJ, 752, 41